Journal of Catalysis xxx (xxxx) xxx

Contents lists available at ScienceDirect

Journal of Catalysis

journal homepage: www.elsevier.com/locate/jcat

Atomically dispersed Pt^{n+} species as highly active sites in Pt/In_2O_3 catalysts for methanol synthesis from CO_2 hydrogenation

Zhe Han [a,b], Chizhou Tang [b], Jijie Wang [b], Landong Li [a], Can Li [b,*]

[a] School of Materials Science and Engineering & National Institute for Advanced Materials, Nankai University, Tianjin 300350, China
[b] State Key Laboratory of Catalysis, Dalian Institute of Chemical Physics, Chinese Academy of Sciences, Dalian 116023, China

ARTICLE INFO

Article history:
Received 12 April 2020
Revised 13 June 2020
Accepted 15 June 2020
Available online xxxx

Keywords:
CO_2 hydrogenation
In_2O_3
Atomically dispersed Pt^{n+} species

ABSTRACT

Hydrogenation of CO_2 into methanol using the H_2 produced from renewable energy is a promising way for carbon capture and utilization. Therefore, the methanol synthesis catalysts with high methanol selectivity are highly desired. In this work, we found that the methanol selectivity of In_2O_3 catalyst can be significantly enhanced by introducing a small amount of Pt. Methanol selectivity can be increased from 72.2% (In_2O_3) to 91.1% (0.58 wt.% Pt/In_2O_3) at 220 °C. The introduced Pt atoms are doped into the In_2O_3, forming atomically dispersed Pt^{n+} species, most of which are stable under working conditions. It is proposed that the atomically dispersed Pt^{n+} species are responsible for the enhanced methanol selectivity, while Pt nanoparticles on In_2O_3 mainly boost the reverse water-gas shift reaction ($CO_2 + H_2 \rightarrow CO + H_2O$).

1. Introduction

The increasing atmospheric CO_2 concentration caused by human activity has become a worldwide concern since CO_2 is considered to be responsible for global climate change and ocean acidification [1–3]. Several routes, such as CO_2 sequestration and conversion of CO_2 into chemicals, have been proposed for the reduction of carbon emission. Utilizing CO_2 as a carbon resource to produce valuable chemicals is more viable. CO_2 can be converted to various chemicals, including methane, olefins, aromatics, and alcohols [4–11]. Methanol is an ideal product since it is a platform molecule for both energy storage and chemical synthesis [12]. There are two major obstacles to be overcome to reduce CO_2 emission by converting CO_2 into methanol. First, the H_2 should be produced utilizing renewable energy instead of fossil resources [13]. Second, highly efficient catalysts for selective hydrogenation of CO_2 into methanol need to be developed.

Ternary $Cu/ZnO/Al_2O_3$ catalyst has been used for the methanol synthesis from syngas (CO and H_2). This catalyst has also been tested for CO_2 hydrogenation [14]. However, $Cu/ZnO/Al_2O_3$ is active in both methanol synthesis reaction and reverse water-gas shift (RWGS) reaction, leading to low methanol selectivity. Unlike CO hydrogenation, a lot of water is generated during CO_2 hydrogenation, causing the sintering of Cu and deactivation of the catalyst. Other catalysts, such as $Cu/ZnO/Ga_2O_3$ [15], Cu/ZrO_2 [16–18], $Cu/ZnO/Al_2O_3/ZrO_2$ [19], Pd/ZnO [20], $Au/CeO_x/TiO_2$ [21], and Ni_5Ga_3/SiO_2 [22] have also been tested with this reaction, confronting with similar problems.

Recently, catalysts based on metal oxides have attracted research attention. For example, $ZnO\text{-}ZrO_2$ solid solution catalyst shows excellent performance in CO_2 hydrogenation for methanol synthesis. This catalyst achieves methanol selectivity up to 86–91% and is very stable under working conditions [23]. Density functional theory (DFT) calculations suggest that the high methanol selectivity is attributed to the simultaneous activation of H_2 and CO_2 on the neighboring Zn^{2+} and Zr^{4+} sites [23]. $CdZrO_x$ and $GaZrO_x$ solid solution catalysts also show good catalytic activity and selectivity to methanol for this reaction [24]. In addition to the ZrO_2 based solid solution catalysts, In_2O_3 was also predicted to be active in CO_2 hydrogenation and possess high selectivity to methanol based on DFT calculations, which have been further demonstrated by experiments [25–29].

Although In_2O_3 catalyst shows higher methanol selectivity compared to $Cu/ZnO/Al_2O_3$, its activity is relatively low. Supporting In_2O_3 on other supports has been investigated to disperse In_2O_3 and improve the activity. However, only a few supported In_2O_3 catalysts such as In_2O_3/ZrO_2 show some limited improvement [28]. A second active metal such as Co [30] and Ni [31] has also been introduced into In_2O_3 to improve the performance. Precious metals are widely used to enhance the catalytic hydrogenation performance of oxide-based catalysts. In this regard, it is reported that introducing Pd nanoparticles prepared separately by a peptide-assisted method into In_2O_3 can improve the methanol synthesis

* Corresponding author.
E-mail address: canli@dicp.ac.cn (C. Li).

https://doi.org/10.1016/j.jcat.2020.06.018
0021-9517/

performance [32]. In another article, the reactivity of Pd in In_2O_3 is found to be related to its state. The low-nuclearity Pd clusters formed in-situ from the isolated Pd atoms in the In_2O_3 lattice improve the methanol synthesis performance without boosting the detrimental RWGS reaction, while Pd nanoparticles mainly promote the RWGS reaction [33]. In addition to Pd, Pt is also reported to improve the performance of In_2O_3 in CO_2 hydrogenation with an inferior improvement compared to Pd in Ref. [33]. However, this article only focuses on the different effects of low-nuclearity Pd clusters and Pd nanoparticles. The detailed state of Pt and the mechanism of the Pt enhancement have not been investigated. Herein, we investigated the effect of Pt on the performance of In_2O_3 in the CO_2 hydrogenation. We found that the addition of a small amount of Pt into In_2O_3 through co-precipitation could increase both the methanol selectivity and the activity in CO_2 hydrogenation. It is affirmed that atomically dispersed Pt^{n+} species is responsible for the improved methanol selectivity while Pt nanoparticles mainly boost the RWGS reaction.

2. Experimental section

2.1. Catalyst preparation

In_2O_3 was prepared following a published method with some modifications [34]. A solution of aqueous NH_4OH (80 mL, 25.0–28.0%, AR, Sinopharm) in ethanol (240 mL, AR, Damao chemical reagent) was added to a solution of $In(NO_3)_3{\cdot}xH_2O$ (27.5 g, 99.99%, Macklin) in a mixture of water (80 mL) and ethanol (240 mL) under vigorous stirring at room temperature. The resulting slurry was immersed into a preheated water bath at 80 °C and stirred for 1 h before cooled to room temperature. The precipitate was separated by centrifugation, washed with water, and dried at 70 °C in air. The resulting solid was calcinated in air for 3 h at 450 °C to obtain the final oxide sample.

Pt/In_2O_3 with Pt loading of 0.03–0.58 wt.% was prepared by co-precipitation. For 0.58 wt.% Pt/In_2O_3, a solution of $(NH_4)_2CO_3$ (15.6 g, AR, Sinopharm) in water (200 mL) was added to a solution of $(NH_4)_2PtCl_6$ (0.7 g, Beijing chemicals factory) and $In(NO_3)_3{\cdot}xH_2O$ (28.6 g, AR, Macklin) in water (300 mL) under vigorous stirring at room temperature. The resulting slurry was immersed into a preheated water bath at 70 °C and stirred for 2 h before cooled to room temperature. The precipitate was separated by centrifugation, washed with water, and dried at 70 °C in air. The resulting solid was calcinated in air for 3 h at 450 °C to obtain the final catalyst sample. For Pt/In_2O_3 with Pt loading between 0.03 wt.% and 0.34 wt.%, the amount of $(NH_4)_2PtCl_6$ and $(NH_4)_2CO_3$ was changed accordingly while other procedures were kept as the same.

The 2.50 wt.% Pt/In_2O_3 and 0.65 wt.% Pt/SiO_2 were prepared by wet impregnation, using platinum nitrate solution (Aladdin, Pt, 18.02%) as the precursor and In_2O_3 or SiO_2 (Aladdin, 99.5%) as supports. The mixture containing Pt precursor, water, and support was dried using a rotary evaporator and calcinated in air for 3 h at 400 °C to obtain the final catalyst.

2.2. Catalyst evaluation

CO_2 hydrogenation was performed using a quartz-lined stainless steel fixed-bed reactor. The catalyst (0.1 g) and quartz sand (0.4 g) were evenly mixed and packed in the reactor. All the catalysts were used directly without any pretreatment. The reactant has the composition of $CO_2/H_2/Ar$ = 24/72/4 (molar ratio). The pressure of the reactor was controlled by a high-temperature back-pressure regulator. Products were analyzed online using gas chromatography (Agilent 7890B). CO_2, Ar, and CO were separated by coupled Porapak N and MolSieve 5A packed columns and quantified by a thermal conductivity detector (TCD). Methane, dimethyl ether, and methanol were separated by an HP-PLOT Q capillary column and quantified by a flame ionization detector (FID). The whole area between the reactor outlet and GC inlet, including the back-pressure valve, transfer lines, and GC sampling valves, was kept at 150 °C to avoid the condensation of the products.

The CO_2 conversion (X) and product selectivity (S) were calculated using the following equations:

$$X(CO_2) = \frac{n(CH_4) + n(CH_3OCH_3) * 2 + n(CH_3OH) + n(CO)}{n(CH_4) + n(CH_3OCH_3) * 2 + n(CH_3OH) + n(CO) + n(CO_2)}$$

$$S(CH_3OH) = \frac{n(CH_3OH)}{n(CH_4) + n(CH_3OCH_3) * 2 + n(CH_3OH) + n(CO)}$$

$$S(CH_4) = \frac{n(CH_4)}{n(CH_4) + n(CH_3OCH_3) * 2 + n(CH_3OH) + n(CO)}$$

$$S(CO) = \frac{n(CO)}{n(CH_4) + n(CH_3OCH_3) * 2 + n(CH_3OH) + n(CO)}$$

where n(P) was the molar flow rate of P in the reactor outlet calculated from peak areas on the chromatogram and relative sensitive factors.

2.3. Catalyst characterization

Powder X-ray diffraction (PXRD) patterns were recorded using a Rigaku D/Max 2500 diffractometer with a Cu rotating anode X-ray source working at 40 kV and 200 mA. The scanning rate was set as 2°/min.

N_2 adsorption-desorption isotherms at liquid nitrogen temperature were measured on a Quantachrome autosorb iQ analyzer. The samples were evacuated at 200 °C for 6 h before measurement.

The Pt content was measured on a PerkinElmer Optima 7300DV ICP-OES spectrometer.

High-resolution transmission electron microscope (HRTEM) and scanning transmission electron microscope (STEM) images were recorded on a JEOL JEM-F200 multi-purpose electron microscope and a JEOL JEM-ARM300F transmission electron microscope.

X-ray photoelectron spectroscopy (XPS) was recorded on a Thermofisher ESCALAB 250Xi instrument with a monochromatic Al Kα X-Ray source. The spectra were calibrated by adjusting C 1s peak to 284.6 eV.

The temperature-programmed reduction with H_2 (H_2-TPR) and temperature-programmed desorption of H_2 (H_2-TPD) were performed using a Quantachrome ChemStar TPx chemisorption analyzer equipped with a TCD detector. For H_2-TPR, the sample was pretreated in Ar at 120 °C for 1 h, then cooled to room temperature, followed by temperature-programmed reduction by 10% H_2/Ar at a ramping rate of 10 °C/min. For H_2-TPD, the sample was heated from room temperature to 300 °C at a ramping rate of 10 °C/min and held at 300 °C for 1 h, followed by cooling to 50 °C in a 10% H_2/Ar mixture. After that, the carrier gas was switched to Ar to remove the weakly adsorbed H_2. Then the temperature was ramping at 10 °C/min for H_2 desorption.

H_2-D_2 isotopic exchange experiment was performed using an AutoChem 2910 chemisorption analyzer (Micromeritics). The sample was pretreated in He at 300 °C for 1 h, followed by cooling to room temperature. Then the treatment gas was switched to mixtures of H_2 and D_2. The temperature was ramping at 5 °C/min. Mass spectrometer (OmniStar) was used to monitor the effluent gas.

Please cite this article as: Z. Han, C. Tang, J. Wang et al., Atomically dispersed Pt^{n+} species as highly active sites in Pt/In_2O_3 catalysts for methanol synthesis from CO_2 hydrogenation, Journal of Catalysis, https://doi.org/10.1016/j.jcat.2020.06.018

3. Results and discussion

3.1. CO_2 hydrogenation on Pt/In_2O_3

A series of Pt/In_2O_3 catalysts containing 0.03–0.58 wt.% Pt were prepared by co-precipitation. For comparison, a Pt/In_2O_3 catalyst with relatively high Pt loading (2.50 wt.%) was also prepared by wet impregnation. The reaction results at 300 °C and 2 MPa are shown in Fig. 1 and Table 1. Methanol and CO are the major products with a small amount of CH_4 (< 0.8%) for all the catalysts. Dimethyl ether (< 0.1%) is also detected when CO_2 conversion is relatively high, which is formed from the dehydration of methanol. For the Pt/In_2O_3 catalysts prepared by co-precipitation, the conversion of CO_2 increases monotonically with Pt loading. The introduction of Pt hardly changes the CH_4 selectivity. In_2O_3 shows a moderate methanol selectivity (48.0%), which is increased to 54.2% upon the introduction of 0.03 wt.% Pt. The highest methanol selectivity (58.4%) is achieved for 0.13 wt.% Pt/In_2O_3. Further increasing the Pt content to 0.34 wt.% and 0.58 wt.% results in a drop of methanol selectivity to 56.8% and 55.8%, respectively. But the methanol selectivity of these two catalysts is still higher than that of In_2O_3. The 2.50 wt.% Pt/In_2O_3 used for comparison shows the lowest methanol selectivity (41.0%), even lower than that of In_2O_3. The significant impact of Pt loading on the methanol selectivity may be related to the different chemical states of the Pt species.

Fig. 2 shows the influence of reaction temperature on the catalytic performance. For all the catalysts, the lowering of reaction temperature leads to a decrease in CO_2 conversion and an increase in methanol selectivity. The CO_2 hydrogenation to methanol is exothermic, while RWGS reaction is endothermic [35]. Therefore, a lower temperature is favorable for methanol synthesis. It is noteworthy that the highest methanol selectivity (91.1%) is achieved for 0.58 wt.% Pt/In_2O_3 at 220 °C, much higher than that of In_2O_3 (72.2%).

The stability of the 0.58 wt.% Pt/In_2O_3 was further tested at 300 °C and 4 MPa (Fig. 3). The stability test results of In_2O_3 are also shown in Fig. 3 for comparison. The relatively low CO_2 conversion for all the catalysts at the first 1 h is due to the instability of the reactor PID temperature controller at the beginning. The CO_2 conversion of In_2O_3 decreases continuously, especially at the initial stage, indicating the deactivation of In_2O_3. The deactivation is caused by the sintering of In_2O_3 due to the product water [29]. The methanol selectivity does not change significantly. The CO_2 conversion of 0.58 wt.% Pt/In_2O_3 also exhibits a slight decrease at the initial 30 h but remains almost the same afterward, suggesting that this catalyst is more stable than In_2O_3. Similar to In_2O_3, the methanol selectivity of 0.58 wt.% Pt/In_2O_3 remains almost unchanged for the time we tested.

Table 1
Reaction results of the catalysts at T = 300 °C, P = 2 MPa, and SV = 24,000 $mL \cdot h^{-1} \cdot g_{cat}^{-1}$.

Catalyst	CO_2 conversion (%)	Product selectivity (%)			
		CO	CH_3OH	CH_4	CH_3OCH_3
In_2O_3	4.4	51.4	48.0	0.6	–
0.03 wt.% Pt/In_2O_3	4.6	45.1	54.2	0.7	–
0.13 wt.% Pt/In_2O_3	5.4	40.9	58.4	0.7	0.01
0.34 wt.% Pt/In_2O_3	6.1	42.6	56.8	0.6	0.02
0.58 wt.% Pt/In_2O_3	6.3	43.6	55.8	0.6	0.02
2.50 wt.% Pt/In_2O_3	8.3	58.6	41.0	0.3	0.01

The influence of space velocity (SV) was investigated using the 0.58 wt.% Pt/In_2O_3 at 300 °C and 4 MPa (Fig. 4). The CO_2 conversion drops with the increase of SV while the methanol selectivity increases. The methanol space-time yield (STY) increases with the SV in the range we tested. The highest methanol space–time yield of 0.76 $g \cdot h^{-1} \cdot g_{cat}^{-1}$ was achieved for this catalyst at SV of 54,000 $mL \cdot h^{-1} \cdot g_{cat}^{-1}$.

3.2. Characterization and discussion

Fig. 5 shows the XRD patterns of the as-prepared catalysts. For In_2O_3, all the diffraction peaks are assigned to cubic In_2O_3 (PDF No. 89-4595). No diffraction peak belongs to the rhombohedral structure is observed, indicating the presence of pure cubic phase of In_2O_3. The diffraction patterns of the as-prepared Pt/In_2O_3 are similar to In_2O_3. There is no diffraction peak belongs to the metallic Pt or Pt oxides phase, suggesting that the particle size of Pt species is smaller than the detection limit of XRD or the Pt species is atomically dispersed in the In_2O_3 lattice. The average crystallite size of the as-prepared catalysts is estimated using the Scherrer equation and shown in Table S1. The as-prepared catalysts have similar average crystallite size (10–12 nm). The specific surface area of these catalysts is determined from N_2 adsorption-desorption isotherms. These catalysts have similar specific surface area (64.5–87.6 $m^2 \cdot g^{-1}$, Table S1).

The TEM images show that the as-prepared 0.58 wt.% Pt/In_2O_3 contains agglomeration of crystals in diameter from ca. 7 nm to 12 nm (Fig. 6a, b, and Fig. S1), in agreement with the average crystallite size estimated from XRD (Table S1). The lattice fringes indi-

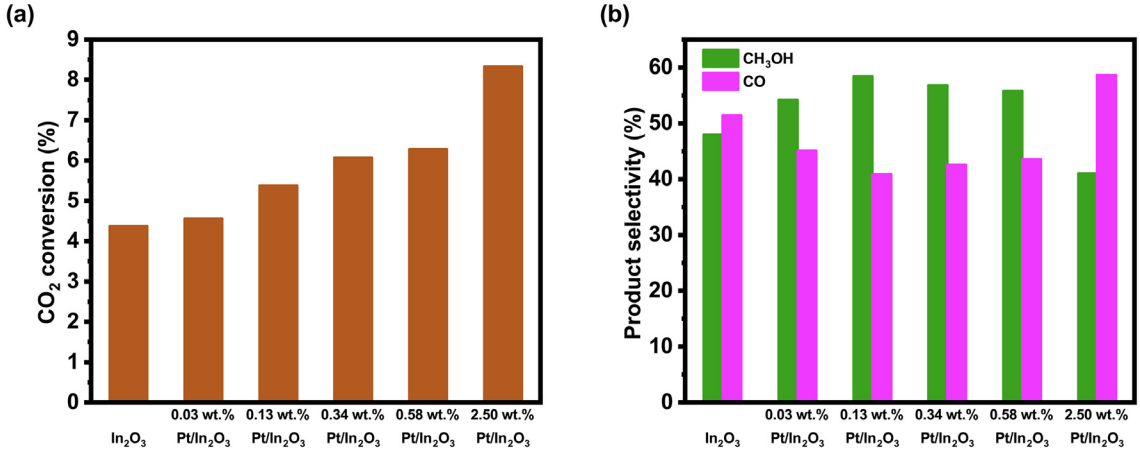

Fig. 1. (a) CO_2 conversion and (b) methanol and CO selectivity of the catalysts. All the catalysts were tested under conditions of T = 300 °C, P = 2 MPa, and SV = 24,000 $mL \cdot h^{-1} \cdot g_{cat}^{-1}$.

Please cite this article as: Z. Han, C. Tang, J. Wang et al., Atomically dispersed Pt^{n+} species as highly active sites in Pt/In_2O_3 catalysts for methanol synthesis from CO_2 hydrogenation, Journal of Catalysis, https://doi.org/10.1016/j.jcat.2020.06.018

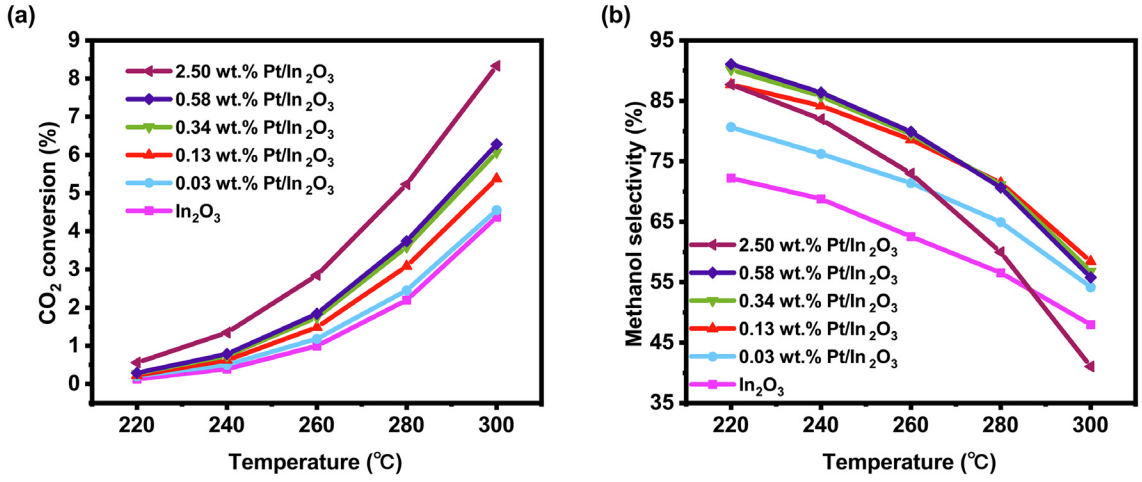

Fig. 2. (a) CO_2 conversion and (b) methanol selectivity at different reaction temperatures. All the catalysts were tested under conditions of P = 2 MPa and SV = 24,000 $mL \cdot h^{-1} \cdot g_{cat}^{-1}$.

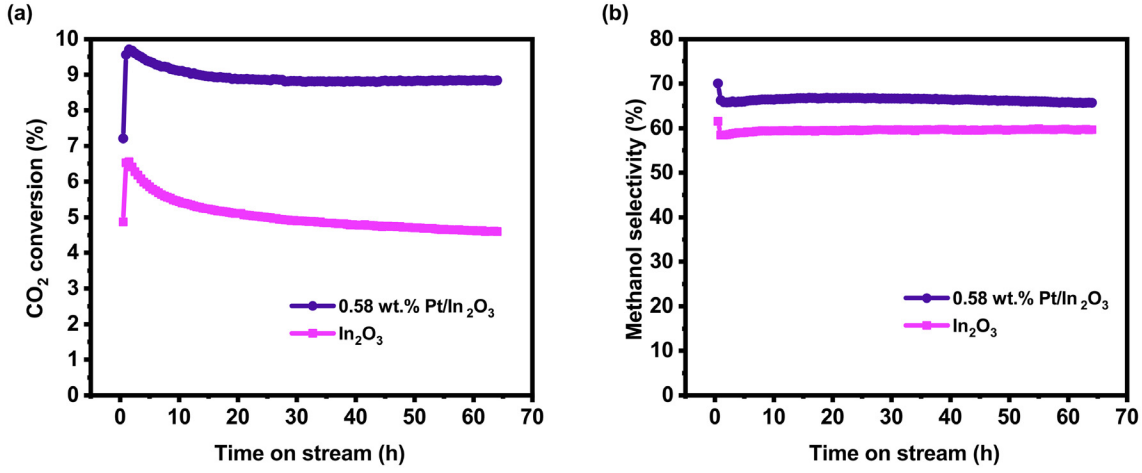

Fig. 3. Stability of the catalysts under conditions of T = 300 °C, P = 4 MPa, and SV = 24,000 $mL \cdot h^{-1} \cdot g_{cat}^{-1}$.

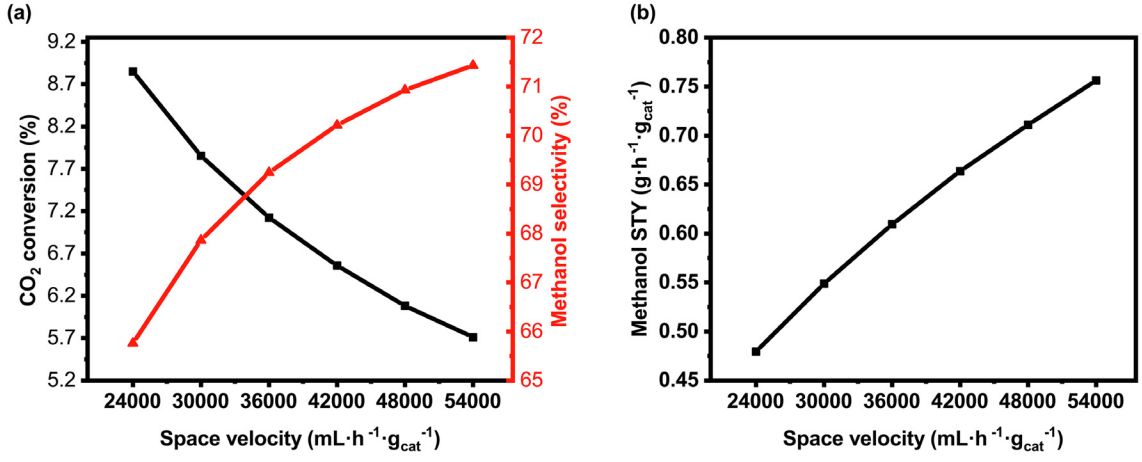

Fig. 4. The influence of space velocity on the (a) CO_2 conversion, methanol selectivity, and (b) methanol space–time yield for 0.58 wt.% Pt/In_2O_3 at T = 300 °C, P = 4 MPa.

cate d spacing of 0.29 nm, corresponding to the (222) planes of cubic In_2O_3, suggesting that these particles are In_2O_3 nanocrystals. Atomic resolution STEM is used to characterize the dispersion of Pt species. There are individual bright spots in the STEM images (Fig. 6b and Fig. S1), indicating that the Pt species are atomically dispersed in In_2O_3. Carefully examination of different regions does

Please cite this article as: Z. Han, C. Tang, J. Wang et al., Atomically dispersed Pt^{n+} species as highly active sites in Pt/In_2O_3 catalysts for methanol synthesis from CO_2 hydrogenation, Journal of Catalysis, https://doi.org/10.1016/j.jcat.2020.06.018

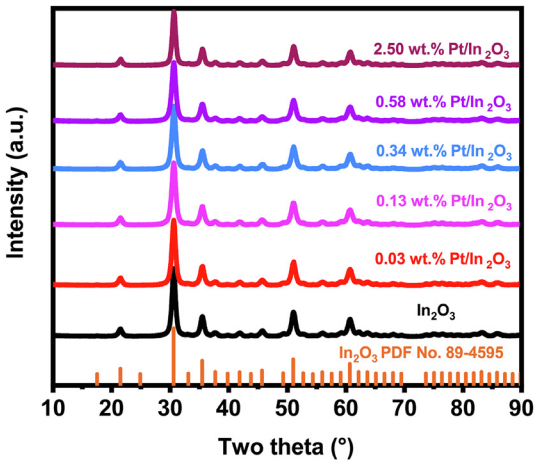

Fig. 5. XRD patterns of the as-prepared In_2O_3 and Pt/In_2O_3.

not show any evidence for the existence of Pt nanoparticles, which should be bright patches in the STEM images if they exist.

The used 0.58 wt.% Pt/In_2O_3 was also studied by TEM. After used in CO_2 hydrogenation, the 0.58 wt.% Pt/In_2O_3 remains to be an agglomeration of small crystals (Fig. 6d, e, and Fig. S2). However, the crystals become larger compared to the catalyst before reaction, implying the sintering of the catalyst during CO_2 hydrogenation, which has also been proved by XRD (Fig. S6). The Pt nanoparticles in diameter of 1–2 nm can be observed in the STEM images of the used 0.58 wt.% Pt/In_2O_3 (Fig. 6e and Fig. S2). These Pt nanoparticles come from the reduction and sintering of the atomically dispersed Pt species during reaction. It should be noted that there is still atomically dispersed Pt species left as revealed by the discrete bright spots in the STEM images (Fig. 6e and Fig. S2), implying that part of the atomically dispersed Pt species is stable against sintering during CO_2 hydrogenation. The TEM images of used 0.13 wt.% Pt/In_2O_3 are shown in Fig. S3 for comparison. Pt nanoparticles with similar size (1–2 nm) are also observed, but their counts are less compared to the used 0.58 wt.% Pt/In_2O_3. Since CO_2 conversion increases while the methanol selectivity drops when the Pt content is increased from 0.13 wt.% to 0.58 wt.% (Fig. 1 and Table 1), the enhanced RWGS reaction should be related to the increasing amount of Pt nanoparticles. The enhancement of RWGS reaction by Pt nanoparticles is further confirmed by the 2.50 wt.% Pt/In_2O_3, which has much more Pt nanoparticles after reaction based on TEM images (Fig. S4) and exhibits the highest CO selectivity.

The chemical states of surface elements were investigated by XPS. The strongest photoelectron peaks of Pt (Pt 4f peaks) overlap with the In 4p peaks, so Pt 4d peaks are used for the identification of the chemical states of Pt. The Pt 4d peaks are not observed for the catalysts with Pt content lower than 0.34 wt.% (Fig. S7a) due to the low content. For 0.34 wt.% Pt/In_2O_3 and 0.58 wt.% Pt/In_2O_3, the Pt $4d_{5/2}$ peak (Fig. 7) can be deconvoluted into two peaks locate at 315.3 eV and 317.0 eV, which belong to Pt^{2+} and Pt^{4+}, respectively [36]. The possibility that Pt species forms separate PtO and PtO_2 phase has been excluded based on XRD and TEM. Therefore, the atomically dispersed Pt species is in the cationic state instead of the metallic state. These Pt^{n+} (Pt^{2+} and Pt^{4+}) cations may replace the In^{3+} ions in the In_2O_3 lattice or locate in the interstitial sites, bonding with the lattice O^{2-} strongly. They may also locate on the defect sites on the surface of In_2O_3. At first sight, the binding energy of Pt $4d_{5/2}$ peak for 2.50 wt.% Pt/In_2O_3 is higher than 0.58 wt.% Pt/In_2O_3. This is caused by the different chemical states

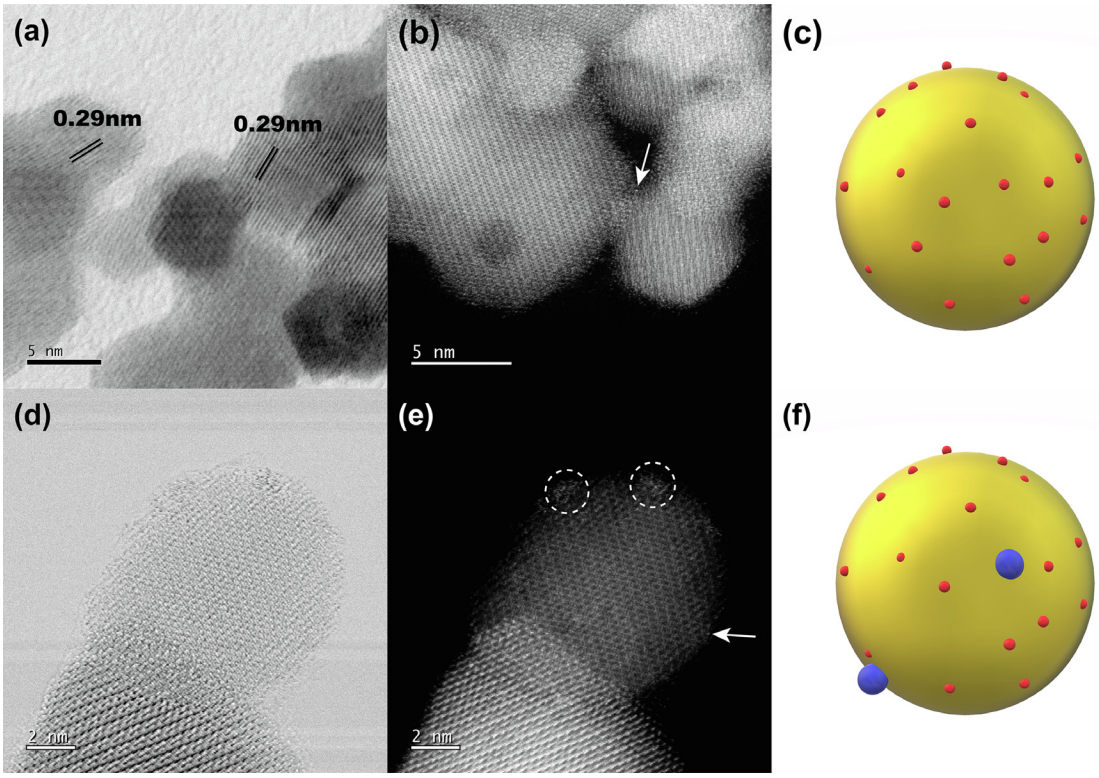

Fig. 6. (a, d) HRTEM and (b, e) STEM images of (a, b) as-prepared 0.58 wt.% Pt/In_2O_3 and (d, e) used 0.58 wt.% Pt/In_2O_3 after reaction. The atomically dispersed Pt species and Pt nanoparticles are marked with arrows and circles, respectively, in the STEM images. Models of the (c) as-prepared 0.58 wt.% Pt/In_2O_3 and (f) used 0.58 wt.% Pt/In_2O_3 are shown on the right side of the STEM images. The yellow ball represents In_2O_3. The red dots and blue patches represent the atomically dispersed Pt species and Pt nanoparticles, respectively.

Please cite this article as: Z. Han, C. Tang, J. Wang et al., Atomically dispersed Pt^{n+} species as highly active sites in Pt/In_2O_3 catalysts for methanol synthesis from CO_2 hydrogenation, Journal of Catalysis, https://doi.org/10.1016/j.jcat.2020.06.018

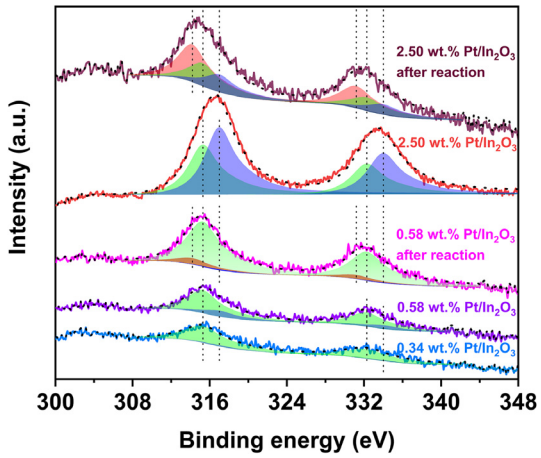

Fig. 7. XPS Pt 4d spectra of the as-prepared catalysts and used catalysts after reaction.

of Pt species. This peak can also be deconvoluted into two peaks at 315.3 eV and 317.0 eV. The first one belongs to Pt^{2+}, while the second one belongs to Pt^{4+}.

The Pt $4d_{5/2}$ peaks of used 0.58 wt.% and 2.50 wt.% Pt/In_2O_3 both shift to lower binding energy, confirming the partial reduction of Pt^{n+} species (Pt^{2+} and Pt^{4+}) during the reaction. The deconvolution results (Table 2) show that about 12.2% of the Pt^{n+} species in 0.58 wt.% Pt/In_2O_3 is reduced to Pt^0 while others are still in atomically dispersed Pt^{n+} state. For 2.50 wt.% Pt/In_2O_3, relatively more Pt^0 (47.9%) is formed compared to 0.58 wt.% Pt/In_2O_3. It should be noted that the used samples were exposed to air before the XPS measurement. Thus, the ratio of Pt^{n+} species for the used catalysts may be overestimated by XPS due to the possible partial oxidation of metallic Pt. However, the existence of atomically dispersed Pt^{n+} species in the used 0.58 wt.% Pt/In_2O_3 has already been demonstrated by atomic resolution STEM. The comparison of TEM images between used 0.58 wt.% and 2.50 wt.% Pt/In_2O_3 also proves that the later sample has more Pt nanoparticles. Considering that the methanol selectivity is enhanced when a small amount of Pt is introduced into In_2O_3, but drops when the Pt loading is higher (Fig. 1 and Table 1), it is reasonable to propose that the atomically dispersed Pt^{n+} species is responsible for the increased methanol selectivity while Pt nanoparticles mainly boost the RWGS reaction.

To further prove that Pt nanoparticles are mainly responsible for the enhanced RWGS reaction, we prepared a Pt/SiO_2 catalyst with Pt loading of 0.65 wt.% by wet impregnation. The catalyst was tested at 300 °C and 2 MPa (reaction conditions same to the conditions used in Fig. 1 and Table 1). This catalyst is active in CO_2 hydrogenation and exhibits very high selectivity to CO (> 99.9%) at a CO_2 conversion of 1.2%. TEM images of the used catalyst (Fig. S5) show plenty of Pt nanoparticles with a wide size distribution range (1–6 nm). The Pt 4f XPS peaks of the used 0.65 wt.% Pt/SiO_2 (Fig. S10) at 70.6 eV ($4f_{7/2}$) and 73.9 eV ($4f_{5/2}$) also clearly indicate that the Pt species in the used 0.65 wt.% Pt/SiO_2 is in the metallic state [37]. Therefore, these results lead us to the conclusion that Pt nanoparticles mainly boost the RWGS reaction.

Table 2
Deconvolution results of the Pt $4d_{5/2}$ XPS peaks.

Sample	Atomic concentration (%)		
	Pt^0 (314.2 eV)	Pt^{2+} (315.3 eV)	Pt^{4+} (317.0 eV)
2.50 wt.% Pt/In_2O_3 after reaction	47.9	29.4	22.7
2.50 wt.% Pt/In_2O_3	0	42.7	57.3
0.58 wt.% Pt/In_2O_3 after reaction	12.2	85.8	2.0
0.58 wt.% Pt/In_2O_3	0	78.9	21.1
0.34 wt.% Pt/In_2O_3	0	92.7	7.3

The binding energy of In $3d_{5/2}$ peak (Fig. S7b) for In_2O_3 is 443.8 eV, implying the +3 oxidation state of In [38]. After adding Pt, the In 3d XPS peaks shift to higher binding energy. This shift is caused by the higher electronegativity of Pt^{n+} (1.513 for Pt^{2+} and 1.880 for Pt^{4+}) than In^{3+} (1.445) [39]. When the In^{3+} ions in the In_2O_3 lattice are replaced by Pt^{n+}, part of the In-O-In structure is replaced by Pt-O-In structure. Electrons transfer from In to Pt through O partially due to the higher electronegativity of Pt^{n+}. The In^{3+} ions become more electron deficient. Therefore, the 3d XPS peaks of In shift to higher binding energy. The shift proves that the interaction between atomically dispersed Pt^{n+} species and In_2O_3 lattice is strong, which may be important in the stabilization of the Pt^{n+} species during CO_2 hydrogenation. The O 1s peaks of all the catalysts are asymmetric (Fig. S7c). This is due to the presence of surface OH groups and oxygen vacancies [40].

The relative surface atomic ratio of Pt and In was calculated from XPS and shown in Table S2. The surface Pt content increases slightly for the 0.58 wt.% Pt/In_2O_3 after reaction, which is caused by the reduction and sintering of part of the atomically dispersed Pt^{n+} species. On the contrary, the surface Pt content for 2.50 wt.% Pt/In_2O_3 decreases after reaction. Since this catalyst is prepared by impregnation, most of the Pt species locate on the surface for the as-prepared catalyst and are reduced to Pt nanoparticles during reaction. The decrease of surface Pt content is due to the migration of In_2O_3 over Pt nanoparticles, which is widely observed for reducible oxides caused by the strong metal support interaction.

H_2-TPR profiles of the as-prepared catalysts are shown in Fig. 8a and Fig. S8. In_2O_3 gives small reduction peaks which start at ca. 120 °C, originating from the creation of surface oxygen vacancies by H_2 reduction. The strong H_2 consumption starts at ca. 430 °C (Fig. S8) is attributed to the reduction of bulk In_2O_3. The reduction peak at ca. 141 °C becomes more significant with the increase of Pt loading for 0.03–0.58 wt.% Pt/In_2O_3 and shifts towards low temperature slightly. This enlarged peak may be attributed to the creation of more oxygen vacancies with more Pt^{n+} species. For 0.34 wt.% and 0.58 wt.% Pt/In_2O_3, a new reduction peak appears at ca. 110 °C, which is probably ascribed to the reduction of Pt^{n+} species on the surface of In_2O_3 and not in the In_2O_3 lattice. Since this part of Pt^{n+} ions locate on the surface of In_2O_3, they are easier to be reduced compared to the Pt^{n+} ions in the In_2O_3 lattice. The reduction of these species results in the formation of Pt nanoparticles. It should be noted that although H_2-TPR shows the reduction of part of the Pt^{n+} species below reaction temperature, the reduction of the atomically dispersed Pt^{n+} species in the In_2O_3 lattice should be harder than this kind of species on the surface due to the strong interaction with In_2O_3 lattice, which has been proved by XPS. On the other hand, the reactant CO_2 and the product H_2O can serve as oxidants for the stabilization of Pt^{n+} species in the oxidation state. The oxidation effect of CO_2 [41] and H_2O [42] under working conditions has been documented in other catalytic systems. For instance, small metallic Co nanoparticles are not stable and prone to be oxidized by H_2O under Fischer-Tropsch synthesis conditions [43]. Metallic Ni in Ni/SiO_2 can be partially oxidized to Ni^{2+} by CO_2 at reaction temperature [41]. In situ EXAFS also demonstrates that part of the metallic Cu is oxidized to Cu^+ and Cu^{2+} during CO_2 hydrogenation on Cu/ZrO_2 [44]. Therefore, not all the Pt^{n+} species are reduced to Pt^0 state during CO_2 hydrogenation, as already proved by XPS and TEM.

The H_2-D_2 isotopic exchange experiment is used to probe the function of Pt in the activation of H_2 (Fig. 8b and Fig. S9). In_2O_3 shows relatively weak ability to catalyze the isotopic exchange of

Please cite this article as: Z. Han, C. Tang, J. Wang et al., Atomically dispersed Pt^{n+} species as highly active sites in Pt/In_2O_3 catalysts for methanol synthesis from CO_2 hydrogenation, Journal of Catalysis, https://doi.org/10.1016/j.jcat.2020.06.018

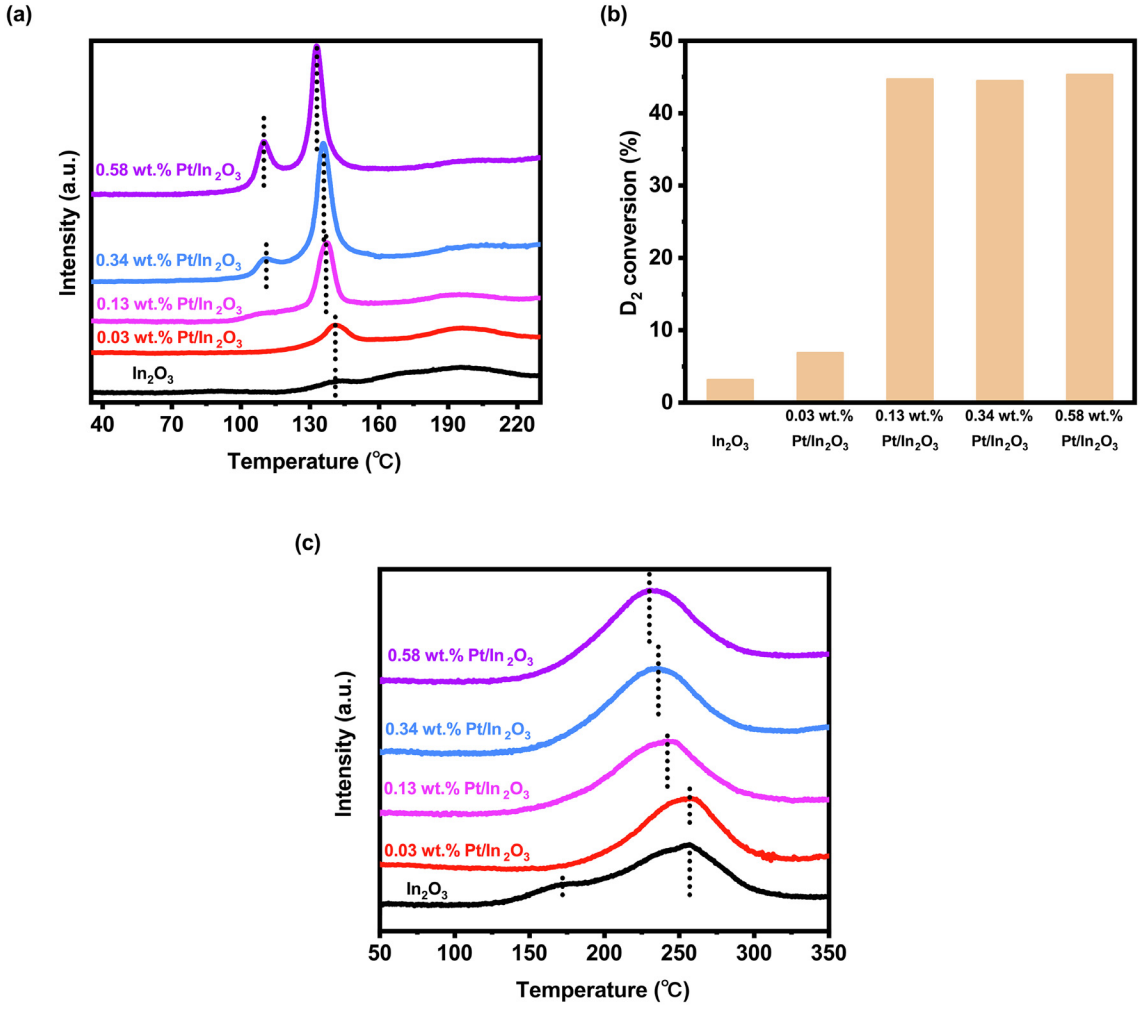

Fig. 8. (a) H_2-TPR profiles, (b) H_2-D_2 exchange results at 100 °C, and (c) H_2-TPD profiles of the catalysts.

H_2 and D_2 at 100 °C with a D_2 conversion of 3%. The D_2 conversion is enhanced to 7% upon the addition of only 0.03 wt.% Pt. The 0.13–0.58 wt.% Pt/In_2O_3 are much more active for the H_2 activation, and all achieve exchange equilibrium at 100 °C. H_2-TPR proves that the reduction of Pt^{n+} species does not happen at 100 °C. Thus, the enhanced ability to activate H_2 can be ascribed to the atomically dispersed Pt^{n+} species. A similar conclusion that the atomically dispersed Pt^{n+} species can facilitate the H_2 activation has also been reported for other Pt-based single-atom catalysts such as Pt on phosphomolybdic acid-modified active carbon (Pt/PMA/C) [45], Pt/m-Al_2O_3 [46], and Pt/FeO_x [47]. The Pt single-atom species in Pt/PMA/C is anchored on the four-fold hollow site on phosphomolybdic acid by coordinating to oxygen atoms and positively charged by electron transfer from Pt to PMA [45]. This catalyst exhibits substantial activity in the hydrogenation of nitrobenzene and cyclohexanone. Similar to Pt/PMA/C, the Pt single-atom species in Pt/m-Al_2O_3 [46] and Pt/FeO_x [47] coordinates with oxygen atoms on the oxide supports and is in oxidized state, which is also active in a variety of hydrogenation reactions.

Fig. 8c shows the H_2-TPD profiles of these catalysts. In_2O_3 and Pt/In_2O_3 exhibit desorption peaks at temperature range between 120 °C and 300 °C. In_2O_3 has two desorption peaks, one main peak centered at ca. 257 °C with a shoulder peak centered at ca. 172 °C. These two peaks belong to H_2 adsorbed on different sites. For 0.03 wt.% Pt/In_2O_3, there is only one desorption peak centered at ca. 257 °C. When the Pt content is increased to 0.13 wt.%, this peak shifts to 242 °C. Further increasing the Pt content makes this peak shift towards low temperature. The shift suggests that H_2 desorbs more easily on Pt/In_2O_3 compared to In_2O_3. The change of H_2-TPD profiles indicates that the introduction of Pt greatly changes the adsorption strength of the adsorbed hydrogen species.

During CO_2 hydrogenation, the surface of In_2O_3 provides an oxygen vacancy containing In_3O_5 structure, serving as a frustrated Lewis pair like structure for the heterolytic dissociation of H_2 [29]. The formed hydride species ($H^{\delta-}$) transfers to the chemisorbed CO_2, results in the formation of formate ($HCOO^-$) intermediate species, which can be further hydrogenated to methanol [29]. The introduction of Pt into In_2O_3 improves both the activity and the methanol selectivity of the catalysts. When Pt was introduced into In_2O_3 by co-precipitation, the positively charged Pt species can be atomically dispersed into the In_2O_3 lattice. During the reaction, part of the Pt species is reduced and sintered, forming Pt nanoparticles. Considering the stability of the 0.58 wt.% Pt/In_2O_3, we propose that most of these Pt nanoparticles are generated at the very initial stage of the reaction. Meanwhile, there are still a significant amount of atomically dispersed Pt^{n+} species remained in the In_2O_3 lattice, which are stabilized by the strong interaction with In_2O_3 lattice and the oxidation effect of CO_2 and product H_2O. The atomically dispersed Pt^{n+} species and Pt nanoparticles are both active in H_2 splitting. H_2 activated on these sites can spill over to the In_2O_3, assisting in the creation of more oxygen vacancies, which are indispensable in CO_2 activation [29]. At the same time,

Please cite this article as: Z. Han, C. Tang, J. Wang et al., Atomically dispersed Pt^{n+} species as highly active sites in Pt/In_2O_3 catalysts for methanol synthesis from CO_2 hydrogenation, Journal of Catalysis, https://doi.org/10.1016/j.jcat.2020.06.018

the atomically dispersed Pt^{n+} species can act as a Lewis acid site and participates in the heterolytic splitting of H_2. This is similar to the heterolytic splitting of H_2 on the oxygen vacancy containing In_3O_5 structure, which may be crucial for the high methanol selectivity of In_2O_3 [29]. Therefore, the methanol selectivity is improved by the atomically dispersed Pt^{n+} species. On the other hand, the formed Pt nanoparticles predominately assist in the homolytic cleavage of H_2 and the formation of CO, which is proved by the comparison of the reaction results between 0.13 wt.% and 0.58 wt.% Pt/In_2O_3 and the high CO selectivity of the reference 2.50 wt.% Pt/In_2O_3 and 0.65 wt.% Pt/SiO_2.

4. Conclusions

In this work, we introduced Pt into In_2O_3 to investigate the role of Pt species in CO_2 hydrogenation. The Pt atoms can be embedded in the lattice of In_2O_3 as atomically dispersed Pt^{n+} species. During CO_2 hydrogenation, part of the positively charged Pt species was reduced and sintered, forming Pt nanoparticles, while others remained in the atomically dispersed, positively charged state. The remaining atomically dispersed Pt^{n+} species and the formed Pt nanoparticles are both active in the activation of H_2 and help to create more oxygen vacancies, on which CO_2 is activated. At the same time, the atomically dispersed Pt^{n+} species that is stable under reaction conditions acts as a Lewis acid site to promote the heterolytic dissociation of H_2 and helps in the methanol formation, while Pt nanoparticles mainly boost the RWGS reaction.

Declaration of Competing Interest

The authors declare that they have no known competing financial interests or personal relationships that could have appeared to influence the work reported in this paper.

Acknowledgments

This work was supported by grants from National Key R&D Program of China (No. 2017YFB0702800), National Natural Science Foundation of China (No. 21802139), and Project of Key Research Plan of Ningxia (2019BDE03003). M. R. Li and N. Ta helped in the electron microscopy measurements.

Appendix A. Supplementary material

Supplementary data to this article can be found online at https://doi.org/10.1016/j.jcat.2020.06.018.

References

[1] P. Friedlingstein, R.M. Andrew, J. Rogelj, G.P. Peters, J.G. Canadell, R. Knutti, G. Luderer, M.R. Raupach, M. Schaeffer, D.P. van Vuuren, C. Le Quéré, Persistent growth of CO_2 emissions and implications for reaching climate targets, Nat. Geosci. 7 (2014) 709–715.
[2] M.R. Allen, D.J. Frame, C. Huntingford, C.D. Jones, J.A. Lowe, M. Meinshausen, N. Meinshausen, Warming caused by cumulative carbon emissions towards the trillionth tonne, Nature 458 (2009) 1163–1166.
[3] J. Hansen, M. Sato, R. Ruedy, K. Lo, D.W. Lea, M. Medina-Elizade, Global temperature change, Proc. Natl. Acad. Sci. 103 (39) (2006) 14288–14293.
[4] M.D. Porosoff, B. Yan, J.G. Chen, Catalytic reduction of CO_2 by H_2 for synthesis of CO, methanol and hydrocarbons: challenges and opportunities, Energy Environ. Sci. 9 (2016) 62–73.
[5] Z. Li, Y. Qu, J. Wang, H. Liu, M. Li, S. Miao, C. Li, Highly selective conversion of carbon dioxide to aromatics over tandem catalysts, Joule 3 (2019) 570–583.
[6] Z. Li, J. Wang, Y. Qu, H. Liu, C. Tang, S. Miao, Z. Feng, H. An, C. Li, Highly selective conversion of carbon dioxide to lower olefins, ACS Catal. 7 (12) (2017) 8544–8548.
[7] Z. You, W. Deng, Q. Zhang, Y. Wang, Hydrogenation of carbon dioxide to light olefins over non-supported iron catalyst, Chin. J. Catal. 34 (2013) 956–963.
[8] Z. Shi, H. Yang, P. Gao, X. Chen, H. Liu, L. Zhong, H. Wang, W. Wei, Y. Sun, Effect of alkali metals on the performance of $CoCu/TiO_2$ catalysts for CO_2 hydrogenation to long-chain hydrocarbons, Chin. J. Catal. 39 (2018) 1294–1302.
[9] X. Liu, M. Wang, C. Zhou, W. Zhou, K. Cheng, J. Kang, Q. Zhang, W. Deng, Y. Wang, Selective transformation of carbon dioxide into lower olefins with a bifunctional catalyst composed of $ZnGa_2O_4$ and SAPO-34, Chem. Commun. 54 (2018) 140–143.
[10] P. Gao, S. Li, X. Bu, S. Dang, Z. Liu, H. Wang, L. Zhong, M. Qiu, C. Yang, J. Cai, W. Wei, Y. Sun, Direct conversion of CO_2 into liquid fuels with high selectivity over a bifunctional catalyst, Nat. Chem. 9 (2017) 1019–1024.
[11] J. Wei, Q. Ge, R. Yao, Z. Wen, C. Fang, L. Guo, H. Xu, J. Sun, Directly converting CO_2 into a gasoline fuel, Nat. Commun. 8 (2017) 15174.
[12] G.A. Olah, Towards oil independence through renewable methanol chemistry, Angew. Chem. Int. Ed. 52 (1) (2013) 104–107.
[13] B.M. Tackett, E. Gomez, J.G. Chen, Net reduction of CO_2 via its thermocatalytic and electrocatalytic transformation reactions in standard and hybrid processes, Nat. Catal. 2 (2019) 381–386.
[14] F. Studt, M. Behrens, E.L. Kunkes, N. Thomas, S. Zander, A. Tarasov, J. Schumann, E. Frei, J.B. Varley, F. Abild-Pedersen, J.K. Nørskov, R. Schlögl, The Mechanism of CO and CO_2 Hydrogenation to Methanol over Cu-Based Catalysts, ChemCatChem 7 (7) (2015) 1105–1111.
[15] M.M.-J. Li, C. Chen, T. Ayvalı, H. Suo, J. Zheng, I.F. Teixeira, L. Ye, H. Zou, D. O'Hare, S.C.E. Tsang, CO_2 hydrogenation to methanol over catalysts derived from single cationic layer CuZnGa LDH precursors, ACS Catal. 8 (5) (2018) 4390–4401.
[16] S. Tada, A. Katagiri, K. Kiyota, T. Honma, H. Kamei, A. Nariyuki, S. Uchida, S. Satokawa, Cu species incorporated into amorphous ZrO_2 with high activity and selectivity in CO_2-to-methanol hydrogenation, J. Phys. Chem. C 122 (10) (2018) 5430–5442.
[17] K. Larmier, W.-C. Liao, S. Tada, E. Lam, R. Verel, A. Bansode, A. Urakawa, A. Comas-Vives, C. Copéret, CO_2-to-methanol hydrogenation on zirconia-supported copper nanoparticles: reaction intermediates and the role of the metal-support interface, Angew. Chem. Int. Ed. 56 (9) (2017) 2318–2323.
[18] K.T. Jung, A.T. Bell, Effects of zirconia phase on the synthesis of methanol over zirconia-supported copper, Catal. Lett. 80 (2002) 63–68.
[19] X. Dong, F. Li, N. Zhao, Y. Tan, J. Wang, F. Xiao, CO_2 hydrogenation to methanol over Cu/Zn/Al/Zr catalysts prepared by liquid reduction, Chin. J. Catal. 38 (2017) 717–725.
[20] H. Bahruji, M. Bowker, G. Hutchings, N. Dimitratos, P. Wells, E. Gibson, W. Jones, C. Brookes, D. Morgan, G. Lalev, Pd/ZnO catalysts for direct CO_2 hydrogenation to methanol, J. Catal. 343 (2016) 133–146.
[21] X. Yang, S. Kattel, S.D. Senanayake, J.A. Boscoboinik, X. Nie, J. Graciani, J.A. Rodriguez, P. Liu, D.J. Stacchiola, J.G. Chen, Low pressure CO_2 hydrogenation to methanol over gold nanoparticles activated on a CeO_x/TiO_2 interface, J. Am. Chem. Soc. 137 (2015) 10104–10107.
[22] F. Studt, I. Sharafutdinov, F. Abild-Pedersen, C.F. Elkjaer, J.S. Hummelshoj, S. Dahl, I. Chorkendorff, J.K. Norskov, Discovery of a Ni-Ga catalyst for carbon dioxide reduction to methanol, Nat. Chem. 6 (2014) 320–324.
[23] J. Wang, G. Li, Z. Li, C. Tang, Z. Feng, H. An, H. Liu, T. Liu, C. Li, A highly selective and stable $ZnO-ZrO_2$ solid solution catalyst for CO_2 hydrogenation to methanol, Sci. Adv. 3 (2017) e1701290.
[24] J. Wang, C. Tang, G. Li, Z. Han, Z. Li, H. Liu, F. Cheng, C. Li, High-performance $MaZrO_x$ (Ma = Cd, Ga) solid-solution catalysts for CO_2 hydrogenation to methanol, ACS Catal. 9 (11) (2019) 10253–10259.
[25] J. Ye, C. Liu, D. Mei, Q. Ge, Active oxygen vacancy site for methanol synthesis from CO_2 hydrogenation on In_2O_3 (110): A DFT Study, ACS Catal. 3 (6) (2013) 1296–1306.
[26] J. Ye, C. Liu, Q. Ge, DFT study of CO_2 adsorption and hydrogenation on the In_2O_3 surface, J. Phys. Chem. C 116 (14) (2012) 7817–7825.
[27] K. Sun, Z. Fan, J. Ye, J. Yan, Q. Ge, Y. Li, W. He, W. Yang, C.-j. Liu, Hydrogenation of CO_2 to methanol over In_2O_3 catalyst, J. CO2 Utiliz. 12 (2015) 1–6.
[28] O. Martin, A.J. Martín, C. Mondelli, S. Mitchell, T.F. Segawa, R. Hauert, C. Drouilly, D. Curulla-Ferré, J. Pérez-Ramírez, Indium oxide as a superior catalyst for methanol synthesis by CO_2 hydrogenation, Angew. Chem. Int. Ed. 55 (21) (2016) 6261–6265.
[29] M.S. Frei, M. Capdevila-Cortada, R. García-Muelas, C. Mondelli, N. López, J.A. Stewart, D. Curulla Ferré, J. Pérez-Ramírez, Mechanism and microkinetics of methanol synthesis via CO_2 hydrogenation on indium oxide, J. Catal. 361 (2018) 313–321.
[30] A. Bavykina, I. Yarulina, A.J. Al Abdulghani, L. Gevers, M.N. Hedhili, X. Miao, A.R. Galilea, A. Pustovarenko, A. Dikhtiarenko, A. Cadiau, A. Aguilar-Tapia, J.-L. Hazemann, S.M. Kozlov, S. Oud-Chikh, L. Cavallo, J. Gascon, Turning a methanation Co catalyst into an In–Co methanol producer, ACS Catal. 9 (8) (2019) 6910–6918.
[31] X. Jia, K. Sun, J. Wang, C. Shen, C.-J. Liu, Selective hydrogenation of CO_2 to methanol over Ni/In_2O_3 catalyst, J. Energy Chem. 50 (2020) 409–415.
[32] N. Rui, Z. Wang, K. Sun, J. Ye, Q. Ge, C.-J. Liu, CO_2 hydrogenation to methanol over Pd/In_2O_3: effects of Pd and oxygen vacancy, Appl. Catal. B: Environ. 218 (2017) 488–497.
[33] M.S. Frei, C. Mondelli, R. García-Muelas, K.S. Kley, B. Puértolas, N. López, O.V. Safonova, J.A. Stewart, D. Curulla Ferré, J. Pérez-Ramírez, Atomic-scale engineering of indium oxide promotion by palladium for methanol production via CO_2 hydrogenation, Nat. Commun. 10 (2019) 3377.
[34] C. Chen, Y. Wei, D. Chen, X. Jiao, Indium oxide nanocrystals: Capping-agent-free synthesis, size-control mechanism, and high gas-sensing performance, Mater. Chem. Phys. 125 (2011) 299–304.

Please cite this article as: Z. Han, C. Tang, J. Wang et al., Atomically dispersed Pt^{n+} species as highly active sites in Pt/In_2O_3 catalysts for methanol synthesis from CO_2 hydrogenation, Journal of Catalysis, https://doi.org/10.1016/j.jcat.2020.06.018

[35] K. Stangeland, H. Li, Z. Yu, Thermodynamic analysis of chemical and phase equilibria in CO_2 hydrogenation to methanol, dimethyl ether, and higher alcohols, Ind. Eng. Chem. Res. 57 (2018) 4081–4094.
[36] J.Z. Shyu, K. Otto, Identification of platinum phases on γ-alumina by XPS, Appl. Surf. Sci. 32 (1988) 246–252.
[37] Y. Duan, S. Song, B. Cheng, J. Yu, C. Jiang, Effects of hierarchical structure on the performance of tin oxide-supported platinum catalyst for room-temperature formaldehyde oxidation, Chin. J. Catal. 38 (2017) 199–206.
[38] C. Donley, D. Dunphy, D. Paine, C. Carter, K. Nebesny, P. Lee, D. Alloway, N.R. Armstrong, Characterization of Indium−Tin oxide interfaces using X-ray photoelectron spectroscopy and redox processes of a chemisorbed probe molecule: effect of surface pretreatment conditions, Langmuir 18 (2002) 450–457.
[39] Y. Zhang, Electronegativities of elements in valence states and their applications. 1. Electronegativities of elements in valence states, Inorg. Chem. 21 (1982) 3886–3889.
[40] L.B. Hoch, T.E. Wood, P.G. O'Brien, K. Liao, L.M. Reyes, C.A. Mims, G.A. Ozin, The rational design of a single-component photocatalyst for gas-phase CO_2 reduction using both UV and visible light, Adv. Sci. 1 (2014) 1400013.
[41] C. Vogt, E. Groeneveld, G. Kamsma, M. Nachtegaal, L. Lu, C.J. Kiely, P.H. Berben, F. Meirer, B.M. Weckhuysen, Unravelling structure sensitivity in CO_2 hydrogenation over nickel, Nat. Catal. 1 (2018) 127–134.
[42] E. van Steen, M. Claeys, M.E. Dry, J. van de Loosdrecht, E.L. Viljoen, J.L. Visagie, Stability of nanocrystals: thermodynamic analysis of oxidation and re-reduction of cobalt in water/hydrogen mixtures, J. Phys. Chem. B 109 (2005) 3575–3577.
[43] N.E. Tsakoumis, J.C. Walmsley, M. Rønning, W. van Beek, E. Rytter, A. Holmen, Evaluation of reoxidation thresholds for γ-Al_2O_3-supported cobalt catalysts under Fischer–Tropsch synthesis conditions, J. Am. Chem. Soc. 139 (10) (2017) 3706–3715.
[44] S.-H. Liu, H.P. Wang, H.-C. Wang, Y.W. Yang, In situ EXAFS studies of copper on ZrO_2 during catalytic hydrogenation of CO_2, J. Electron Spectrosc. Related Phenomena 144-147 (2005) 373–376.
[45] B. Zhang, H. Asakura, J. Zhang, J. Zhang, S. De, N. Yan, Stabilizing a $Platinum_1$ Single-Atom Catalyst on Supported Phosphomolybdic Acid without Compromising Hydrogenation Activity, Angew. Chem. Int. Ed. 55 (29) (2016) 8319–8323.
[46] Z. Zhang, Y. Zhu, H. Asakura, B. Zhang, J. Zhang, M. Zhou, Y. Han, T. Tanaka, A. Wang, T. Zhang, N. Yan, Thermally stable single atom Pt/m-Al_2O_3 for selective hydrogenation and CO oxidation, Nat. Commun. 8 (2017) 16100.
[47] H. Wei, X. Liu, A. Wang, L. Zhang, B. Qiao, X. Yang, Y. Huang, S. Miao, J. Liu, T. Zhang, FeO_x-supported platinum single-atom and pseudo-single-atom catalysts for chemoselective hydrogenation of functionalized nitroarenes, Nat. Commun. 5 (2014) 5634.

Please cite this article as: Z. Han, C. Tang, J. Wang et al., Atomically dispersed Pt^{n+} species as highly active sites in Pt/In_2O_3 catalysts for methanol synthesis from CO_2 hydrogenation, Journal of Catalysis, https://doi.org/10.1016/j.jcat.2020.06.018